Mutual-Coupling in High-Q Silicon Dual-Concentric Micro-Ring/Racetrack Resonator

Yan Xu, Tingyu Liu, Songyue Liu, Xiaoqiang Sun, *Member, IEEE*, and Daming Zhang

***Abstract*—Micro-ring resonator (MRR) is a key element in integrated optics. The mutual-coupling in dual-concentric MRR has great influence on the resonance output. In this work, high-Q silicon dual-concentric MRR and racetrack resonator have been investigated by the coupled mode theory. The theoretical model is built to explain and alleviate the phenomenon of resonance splitting. CMOS fabrication is adopted for the preparation of dual-concentric MRR and racetrack resonators. The highest Q-factors of dual-concentric MRR and racetrack resonator are measured to be $\sim$9.00 $\times$ 10^4 at 1530.783 nm and $\sim$7.32 $\times$ 10^4 at 1536.596 nm, respectively. The notch depth improvement over 20 dB has been demonstrated on the 5-μm-radius double-ring structure. The experimental results prove that the asymmetry of resonance splitting can be tuned by adjusting the distance between the inner-ring and outer-ring, as well as the waveguide width. The proposed work has potentials in the design and optimization of dual-concentric ring resonators.**

***Index Terms*—Micro-ring resonator, racetrack resonator, silicon photonics, CMOS.**

I. Introduction

DRIVEN by the demand of new-generation communication and large-scale computing, such as big data, cloud computing, the Internet of Things, artificial intelligence and so on, the silicon photonics has become an attractive and promising solution due to its advantages of small size, low cost and high integration. Basic silicon waveguide components have applications in sensors [1], [2], filters [3], [4], optical switches/modulators [5]–[7], [8], delayer [9], [10], polarization/wavelength/mode (de)multiplexer [11]–[13], and so on. Though have been well investigated, silicon photonics still deserves further study to explore its potentials and applications in broader fields. Among the typical components, micro-ring resonators (MRR) with characteristics of small size and wavelength selectivity have been widely used in different functional devices.

As one of the key parameters of MRR, Q factor (Q = λ / FWHM, λ is resonance wavelength) is an important characteristic to evaluate the performance. To increase Q factor, subwavelength grating-based micro-ring resonators have been experimentally studied. The MRR with a radius of 5 μm has trapezoidal silicon pillars, exhibiting an applicable quality factor of 1.15 $\times$ 10^4 [14]. When this MRR combines working with the local weak gratings, a high Q factor of 1.90 $\times$ 10^4 still remains [15]. The dual-ring resonator (DRR) shows favorable resonance, too. For example, the Q factor of the inner ring (with a radius of 5 μm) of a DRR is around 3.70 $\times$ 10^4 [16]. DRR have been applied in sensor [17] and filter [18]. However, the phenomenon of resonance splitting may occur if the mutual mode coupling between two resonators is too much strong [19]. To correctly deal with such mutual-coupling and resonance splitting, an accurate and robust model for the analysis of dual-concentric ring resonator is demanded. However, current fitting models can only describe the symmetrical resonance splitting or the single-ring case [20]–[24]. As far as we know, no appropriate models for the analysis of asymmetric resonances splitting in the dual-concentric ring resonator.

In this work, the coupled mode theory is adopted to study the cause of resonance splitting. Two-dimensional finite-difference time-domain (2D-FDTD) calculations are adopted to predict and explain the phenomenon of resonance splitting. The experimental characterizations on the asymmetric resonance confirm the validity of proposed model on the analysis of dual-concentric ring resonators. The resonance status can be adjusted by tuning the geometric parameters of the inner and outer rings. The proposed model has application in the design optimization of dual concentric-ring resonators.

II. Principle and Structure

The well-known add-drop MRR structures have been widely used in different applications [25]–[30]. Compared with the all-pass structure, the introduction of another straight waveguide will lead to an excess coupling, which complicates the theoretical analysis and demands massive memories and time for calculations. Since the main purpose of this work is to analyze the resonance splitting in dual-concentric ring resonators, the adoption of all-pass ring structure is adequate to construct the theoretical model and provides enough data. Therefore, the all-pass structure is used in this study.

The schematic of dual-concentric silicon waveguide MRR and racetrack resonator are shown in Fig. 1(a) and (b), respectively. Both consist of the concentric silicon ring/racetrack and the bus waveguide. Here, the 220 nm-thick silicon waveguide is surrounded by the 3 μm-thick SiO_2 lower and upper-claddings. Lightwave propagating from the left to right (S_{in}) in the

Manuscript received 1 April 2022; revised 29 May 2022; accepted 24 June 2022. Date of publication 28 June 2022; date of current version 12 July 2022. This work was supported by the National Key Research and Development Program of China under Grant 2019YFB2203001. *(Corresponding author: Xiaoqiang Sun.)*

The authors are with the State Key Laboratory of Integrated Optoelectronics, College of Electronic Science & Engineering, Jilin University, Changchun 130012, China (e-mail: xyan17@mails.jlu.edu.cn; liuty20@mails.jlu.edu.cn; syliu20@mails.jlu.edu.cn; sunxq@jlu.edu.cn; zhangdm@jlu.edu.cn).

Digital Object Identifier 10.1109/JPHOT.2022.3186914

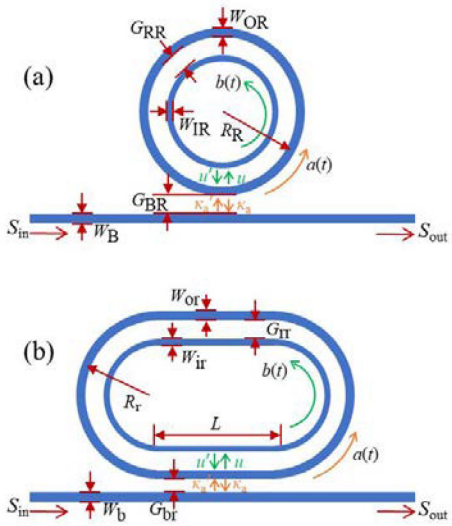

Fig. 1. Schematic of dual-concentric (a) MRR and (b) Racetrack resonator that is side-coupled to a straight bus waveguide. Lightwave propagating from the left to right (S_{in}) in the waveguide only generates the counter-clockwise travelling mode $a(t)$ in the outer-ring. Counter-clockwise travelling mode $b(t)$ in the inner-ring can only be generated by evanescent directional coupling from $a(t)$.

waveguide only generates the counter-clockwise travelling mode $a(t)$ in the outer-ring. Counter-clockwise travelling mode $b(t)$ in the inner-ring can only be generated by the evanescent directional coupling from $a(t)$.

Since the principle of dual-concentric MRR is the same to that of the dual-concentric racetrack resonator, then we take the analysis of dual-concentric MRR as an example. The amplitudes of resonant mode in the outer-ring and inner-ring are denoted as a(t) and b(t), respectively. The traveling waves of a and b are given by [21], [31]

$$\frac{da}{dt} = \left[j\omega_{\mathrm{a}} - \frac{1}{\tau_{\mathrm{a}}}\right] \mathrm{a} - j\kappa_{\mathrm{a}} S_{\mathrm{in}} - jub, \tag{1}$$

$$\frac{db}{dt} = \left[j\omega_{\mathrm{b}} - \frac{1}{\tau_{\mathrm{b}}}\right] b - ju\prime a. \tag{2}$$

Among which S_{in} is the amplitude of incident light. The amplitude of lightwave at the output port S_{out} can be described by [32]

$$S_{\mathrm{out}} = S_{\mathrm{in}} - j\kappa'_{\mathrm{a}} a. \tag{3}$$

The power transfer function T(ω) based on (1), (2) and (3) can be described by

$$\mathrm{T}(\omega) = \left|\frac{S_{\mathrm{out}}}{S_{\mathrm{in}}}\right|^2 = \left|1 - \frac{|\kappa_{\mathrm{a}}\kappa'_{\mathrm{a}}|\left[j(\omega-\omega_{\mathrm{b}}) + \frac{1}{\tau_{\mathrm{b}}}\right]}{\left[j(\omega-\omega_{\mathrm{a}}) + \frac{1}{\tau_{\mathrm{a}}}\right]\left[j(\omega-\omega_{\mathrm{b}}) + \frac{1}{\tau_{\mathrm{b}}}\right] + uu'}\right|^2. \tag{4}$$

In the dual-concentric MRR, no directional coupling between bus waveguide and inner-ring exists. The separations of the waveguide to ring and the inner-ring to outer-ring, are well set for the coupling of waveguide mode to specific traveling mode in the outer-ring. The coupling coefficients of outer-ring/waveguide (waveguide/outer-ring) and outer-ring/inner-ring (inner-ring/outer-ring) are defined as κ_{a} (κ'_{a}) and u (u'), respectively. For simplicity, a dimensionless factor f is introduced to mathematically describe the coupling among inner-ring, outer-ring and bus waveguide. Therefore, we have

$$\kappa'_{\mathrm{a}} = f_{k_{\mathrm{a}}} \tag{5-1}$$

$$u' = fu \tag{5-2}$$

It should be noted that f may be complex, for example, only representing a phase difference between the inner- and outer-rings coupling. u that is merely a value manifesting the mutual coupling rate of two traveling modes in rings, relates to no power loss in the whole system. Hence, there exists two possible cases in the dual-concentric MRR. One is the ideal case ($f = 1$), another is the common case ($f \neq 1$).

A. Ideal Case

When $f = 1$, the Eq. (4) changes to [17], [21], [33]

$$\mathrm{T}(\omega) = \left|\frac{S_{\mathrm{out}}}{S_{\mathrm{in}}}\right|^2 = \left|1 - \frac{|\kappa_{\mathrm{a}}|^2\left[j(\omega-\omega_{\mathrm{b}}) + \frac{1}{\tau_{\mathrm{b}}}\right]}{\left[j(\omega-\omega_{\mathrm{a}}+u) + \frac{1}{\tau_{\mathrm{a}}}\right]\left[j(\omega-\omega_{\mathrm{b}}-u) + \frac{1}{\tau_{\mathrm{b}}}\right]}\right|^2, \tag{6}$$

where ω_{a} and ω_{b} are resonant frequencies of the outer- and inner-rings, respectively. τ is the photon life time. The reciprocal photon life time that complies with the decay rate $1/\tau$ relates to the power coupling to waveguide ($1/\tau_{\mathrm{e}}$) and the power dissipation due to the intrinsic losses ($1/\tau_{\mathrm{i}}$). Here, we have

$$\frac{1}{\tau} = \frac{1}{\tau_{\mathrm{e}}} + \frac{1}{\tau_{\mathrm{i}}}. \tag{7}$$

The relationship between the outer-ring/waveguide coupling coefficient κ_{a} and the power dissipation rate τ_{ae} can be expressed by $|\kappa_{\mathrm{a}}|^2 = 2/\tau_{\mathrm{ae}}$. To zero T($\omega$), the real part and imaginary part of T(ω) are both supposed to be zero if the incident optical frequencies satisfy the resonance frequencies. Two occasions ($u = 0$ and $u \neq 0$) may bring T(ω) to zero, which corresponds to the critical-coupling.

When $u = 0$, the Eq. (6) changes to

$$\omega = \omega_{\mathrm{a}} = \omega_{\mathrm{b}}, \tag{8-1}$$

$$\frac{1}{\tau_{\mathrm{ai}}} = \frac{1}{\tau_{\mathrm{ae}}}. \tag{8-2}$$

When $u \neq 0$, the Eq. (6) changes to

$$\mathrm{Re}(\mathrm{T}) = \frac{1}{\tau_{\mathrm{a}}\tau_{\mathrm{b}}} - \frac{|\kappa_{\mathrm{a}}^2|}{\tau_{\mathrm{b}}} + u^2 = 0, \tag{9-1}$$

$$\mathrm{Im}(\mathrm{T}) = \frac{\omega-\omega_{\mathrm{a}}}{\tau_{\mathrm{b}}} + \frac{\omega-\omega_{\mathrm{b}}}{\tau_{\mathrm{a}}} - |\kappa_{\mathrm{a}}^2|(\omega-\omega_{\mathrm{b}}) = 0. \tag{9-2}$$

Alternatively, (9-1) can be expressed as

$$u^2 = \left|\frac{1}{\tau_{\rm b}}\left(\frac{2}{\tau_{\rm ae}} - \frac{1}{\tau_{\rm a}}\right)\right| = \left|\frac{1}{\tau_{\rm b}}\left(\frac{1}{\tau_{\rm ae}} - \frac{1}{\tau_{\rm ai}}\right)\right|, \tag{10-1}$$

Here, u is an optimal value $u_{\rm m}$. Similarly, (9-2) changes to

$$\omega = \omega_{\rm a} = \omega_{\rm b}. \tag{10-2}$$

When $a(t)$ is close to $b(t)$, which gives $\frac{1}{\tau_{\rm a}} = \frac{1}{\tau_{\rm b}}$, (9-1) may be described as

$$u_{\rm m}^2 = \left|\frac{1}{\tau_{\rm ae}^2} - \frac{1}{\tau_{\rm ai}^2}\right|. \tag{11}$$

Consequently, the resonant frequencies of the outer-ring and inner-ring should almost be the same. The coupling loss to the waveguide ($1/\tau_{\rm ae}$) should be equal to the intrinsic loss ($1/\tau_{\rm ai}$), or satisfy the definition in (11). When u infinity approaches to zero, (6) is simplified to the case of a single ring that is without mutual-coupling.

According to Eq. (6), assuming the resonance splitting occurs, two symmetric resonances are supposed to have the same notch depth, which is in accordance to the reports in Ref [21] and [22]. Since over 80% resonance splitting are practically asymmetric [31], it is more desirable to study the power transfer under the common case.

B. Common Case

Based on above analysis and hypothesis, the resonant frequency and the loss of inner-ring is the same to that of the outer, which gives $\omega_0 = \omega_{\rm a} = \omega_{\rm b}$ and $\frac{1}{\tau_{\rm a}} = \frac{1}{\tau_{\rm b}} = \frac{1}{\tau_{\rm ae}} + \frac{1}{\tau_{\rm ai}}$. The operation in common case is the same to that in the ideal case, except for $f \neq 1$. Hence, (4) is rewritten to be

$$\mathrm{T}\ (\omega) = \left|\frac{S_{\rm out}}{S_{\rm in}}\right|^2 = \left|1 - \frac{f\kappa_{\rm a}^2}{2}\left[\frac{1}{{\rm j}\,(\omega - \omega_0 + f u\,) + \frac{1}{\tau_{\rm ae}} + \frac{1}{\tau_{\rm ai}}} + \frac{1}{{\rm j}\,(\omega - \omega_0 - u) + \frac{1}{\tau_{\rm ae}} + \frac{1}{\tau_{\rm ai}}}\right]\right|^2. \tag{12}$$

The resonance-splitting in common case is the same as the ideal case, too. Here, u is an important factor to determine if the resonance-splitting happens. Comparing (12) with (6), f also has great contribution. When the resonance-splitting occurs, the frequency offset in the imaginary part is affected by both u and f. Due to the impact of f, there exist different phases about the splitting resonant frequency. Different decay of resonant strength can be observed, too.

Based on the analysis on the ideal and common cases, it is a rare scenario to satisfy the requirement of critical-coupling. The more easily happened under-coupling ($\frac{1}{\tau_{\rm ae}} < \frac{1}{\tau_{\rm ai}}$) and over-coupling ($\frac{1}{\tau_{\rm ae}} > \frac{1}{\tau_{\rm ai}}$) make the experimental implementation of critical-coupling become a critical challenge. To be noted, the presence of mutual mode coupling is helpful to construct the critical-coupling and deepens the notch depth [21]. However, the single resonance notch will split into two when u is over $u_{\rm m}$, no matter it is under-coupling or over-coupling [22]. As mentioned above, it is likely to miss the critical-coupling and fail the complete channel drop. Nevertheless, by changing the gap width between the inner- and outer-ring, u can be adjusted to increase notch depth or decrease the 3-dB bandwidth when widths of ring/bus waveguide are fixed in all cases. In other words, the mutual coupling offers another freedom for high-Q resonator design since there exist hardship of high-precise fabrication and the limitation of minimum line width. As one of the reasons leading to asymmetric resonance-splitting, the quantitative and qualitative analysis on f becomes a critical issue.

III. Simulations

2D-FDTD is adopted in the resonance analysis. To be noted, the impact of f on the formation of asymmetric resonance-splitting is hard to be distinguished with 2D-FDTD simulations, because the coupling between bus waveguide and MRR has already been considered in Maxwell's equations. On the other hand, through changing the distance between the inner-ring and outer-ring, the influence of u on the resonance of dual-concentric MRR and racetrack resonator can be confirmed by 2D-FDTD simulations.

At the input port, the fundamental TE mode is coupled into the bus waveguide. The initial structure parameters of dual-concentric ring resonator are set as following: bus waveguide width $W_{\rm B} = 0.30\ \mu$m, bus/outer-ring waveguide separation $G_{\rm BR} = 0.40\ \mu$m, outer-ring waveguide width $W_{\rm OR} = 0.40\ \mu$m, outer/inner-ring waveguide separation $G_{\rm RR} = 0.40\ \mu$m, inner-ring waveguide width $W_{\rm IR} = 0.40\ \mu$m, and outer-ring radius $R_{\rm R} = 5\ \mu$m. The initial structure parameters of dual-concentric racetrack resonator are set as following: bus waveguide width $W_{\rm b} = 0.40\ \mu$m, bus/outer-ring waveguide separation $G_{\rm br} = 0.40\ \mu$m, outer-ring waveguide width $W_{\rm or} = 0.40\ \mu$m, outer/inner-ring waveguide separation $G_{\rm rr} = 0.52\ \mu$m, inner-ring waveguide width $W_{\rm ir} = 0.30\ \mu$m, outer-ring radius $R_{\rm r} = 5\ \mu$m and coupling length $L = 10\ \mu$m.

A. Dual-Concentric Ring Resonator

In this work, the radii of inner-ring and outer-ring are approximately 4 μm and 5 μm, respectively. The relationship between the radius of inner-ring and the separation between two concentric rings satisfies $R_{\rm R} - G_{\rm RR} \geq 10 \times G_{\rm RR}$. Hence, two counter-clockwise modes are supposed to share the same resonance frequency and decay rate. In this way, the mode propagation in the dual-concentric MRR coincides with the analysis in Section II.

To investigate the contribution of u to the resonance, the transmission at output port $S_{\rm out}$ is calculated with above mentioned geometric parameters. As shown in Fig. 2, the increment of rings gap $G_{\rm RR}$ could effectively alleviate the phenomenon of resonance splitting, meanwhile, enhancing the notch depth till $G_{\rm RR}$ reaches to 0.38 μm (blue line). When $G_{\rm RR}$ further increases to 0.60 μm, the single resonance inclines to splitting again. This can be explained that the enlargement of $G_{\rm RR}$ leads to the failure of hypothesis, which implies $R_{\rm R} - G_{\rm RR} < 10 \times G_{\rm RR}$. The inner-ring and outer-ring have different resonance frequencies (or wavelength) and decay rate. In other words, the extreme small radius of dual-concentric MRR fails the method of increasing $G_{\rm RR}$ to mitigate the unfavorable resonance splitting. According

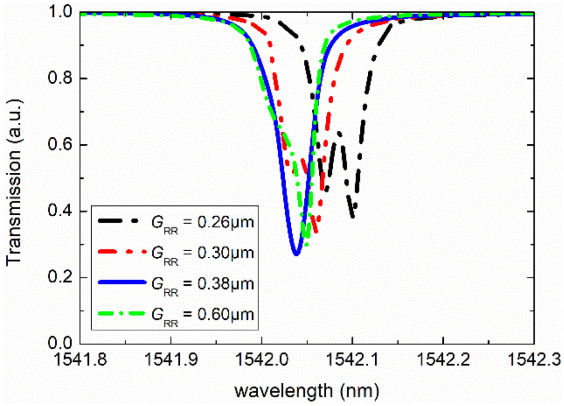

Fig. 2. Normalized transmission of dual-concentric MRR at different G_{RR}, when $W_{\mathrm{B}} = 0.30\ \mu$m, $G_{\mathrm{BR}} = 0.40\ \mu$m, $W_{\mathrm{OR}} = 0.40\ \mu$m, $W_{\mathrm{IR}} = 0.40\ \mu$m, $R_{\mathrm{R}} = 5\ \mu$m.

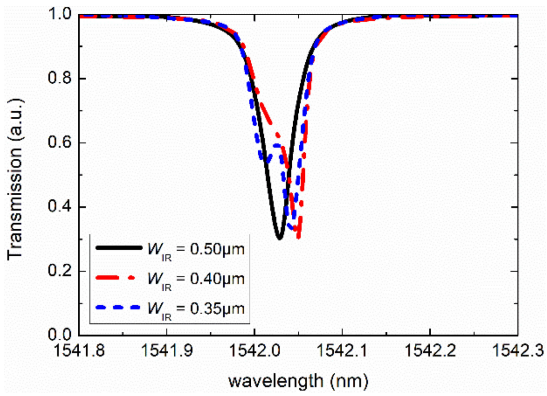

Fig. 3. Normalized transmission of dual-concentric MRR at different inner-ring waveguide widths, when geometric parameters are set as $W_{\mathrm{B}} = 0.30\ \mu$m, $G_{\mathrm{BR}} = 0.40\ \mu$m, $W_{\mathrm{OR}} = 0.40\ \mu$m, $G_{\mathrm{RR}} = 0.60\ \mu$m, and $R_{\mathrm{R}} = 5\ \mu$m.

to our simulations, no apparent resonance splitting will happen at $G_{\mathrm{RR}} = 0.38\ \mu$m, if the fabrication error is less than 40 nm. Besides, the change of G_{RR} causes the fluctuation of resonance notch depth and the shift of resonance wavelength. This partly originates from the 2D-FDTD calculations, in which the interested region is divided into millions of Yee cells. As a result, the electromagnetic field may become unstable when G_{RR} has been changed.

According to the micro-ring resonance condition

$$\mathrm{m}\lambda = 2\pi R \times n_{\mathrm{eff}}, \tag{13}$$

the resonance wavelength λ is proportional to the radius R of the ring and the effective index of waveguide n_{eff}. The method of enlarging G_{RR} implies the reduction of inner ring radius, which will bring the blueshift of resonance wavelength. To guarantee the resonance of dual-concentric MRR and compensate the wavelength shifting, higher effective index is demanded by the adoption of wider inner-ring waveguide. Fig. 3 shows the normalized transmission of dual-concentric MRR when W_{IR} is 0.35 μm, 0.40 μm and 0.50 μm. In this case, other geometric parameters are fixed as $W_{\mathrm{B}} = 0.30\ \mu$m, $G_{\mathrm{BR}} = 0.40\ \mu$m, $W_{\mathrm{OR}} = 0.40\ \mu$m, $G_{\mathrm{RR}} = 0.60\ \mu$m, and $R_{\mathrm{R}} = 5\ \mu$m. Obviously,

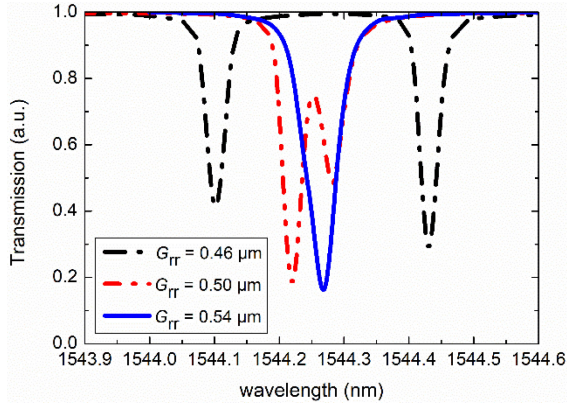

Fig. 4. Normalized transmission of dual-concentric racetrack resonator at different gap widths, when geometric parameters are set as $W_{\mathrm{b}} = 0.40\ \mu$m, $G_{\mathrm{br}} = 0.40\ \mu$m, $W_{\mathrm{or}} = 0.40\ \mu$m, $W_{\mathrm{ir}} = 0.30\ \mu$m, $R_{\mathrm{r}} = 5\ \mu$m and $L = 10\ \mu$m.

the wider W_{IR} could effectively ameliorate the symmetry of resonance-splitting transmission.

B. Dual-Concentric Racetrack Resonator

Similar analysis method is applied to the study of dual-concentric racetrack resonator. As shown in Fig. 4, the increment of rings gap G_{rr} from 0.46 to 0.54 μm, which corresponds to the reduction of u, effectively alleviates the resonance-splitting of transmission spectrum, and the symmetric resonance is observed. Moreover, the resonance strength has also been enhanced by the G_{rr} increment, because a larger G_{rr} weakens the mutual-coupling between the inner-ring and outer-ring, leading to the approaching of u and u' to the optimal u_{m}. In fact, for the case that u or u' is less than u_{m}, no resonance-splitting is observed till G_{rr} is larger than 0.50 μm.

As shown in Fig. 4, the notch depth of spectrum with no splitting is larger than that of the spectrum with resonance splitting in the racetrack resonator. Besides, a narrower bandwidth can be observed in the spectrum with no splitting. As has been reported [22], the anomalous dispersion happens and the mutual-coupling lowers the resonance notch depth in the transmission spectrum, if $\frac{1}{\tau_{\mathrm{e}}} < \frac{1}{\tau_{\mathrm{i}}}$ and resonator is in the under-coupling status. In case $\frac{1}{\tau_{\mathrm{e}}} > \frac{1}{\tau_{\mathrm{i}}}$, the resulted over-coupling will lead to the resonance-splitting. The anomalous dispersion that accompanies with the enhancement of mutual-coupling deepens the notch of splitting. To be noted, the contribution of G_{RR} or G_{rr} to resonance that is represented by u is investigated by 2D-FDTD simulation. Its correctness will be verified in the following experiment results discussion.

IV. Experiment and Discussion

To verify the proposed theoretical model, dual-concentric MRR and racetrack ring with different geometric parameters have been prepared with CMOS fabrication. The proposed resonators were constructed on a commercial SOI wafer with the 220-nm top silicon layer and 3-μm thick buried silicon oxide. Firstly, photoresist was spin-coated onto the top silicon layer and cured. The waveguide and grating coupler patterns

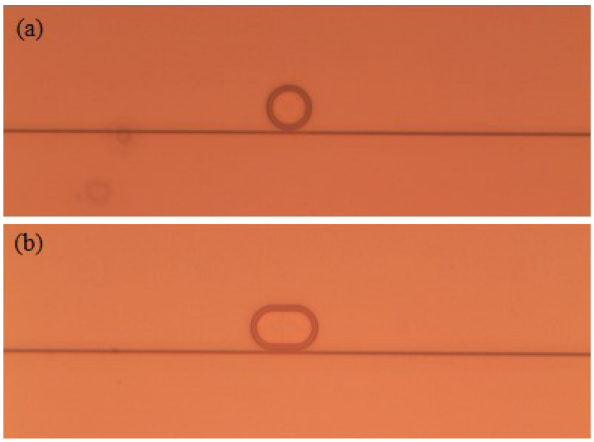

Fig. 5. Optical microscope image (×1000) of (a) Dual-concentric MRR, and (b) Dual-concentric racetrack resonator.

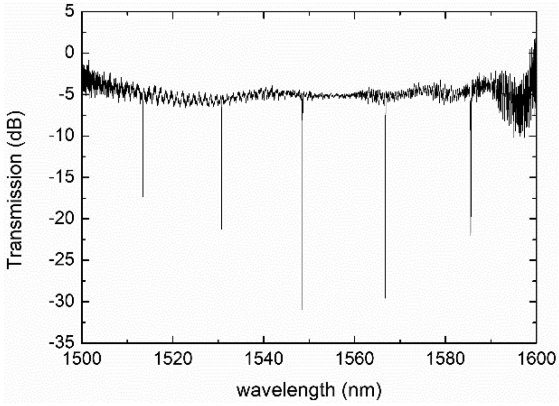

Fig. 6. Measured transmission spectrum of dual-concentric MRR as a function of optical wavelength, when $W_{\mathrm{B}} = 0.30\ \mu$m, $G_{\mathrm{BR}} = 0.40\ \mu$m, $W_{\mathrm{OR}} = 0.40\ \mu$m, $G_{\mathrm{RR}} = 0.40\ \mu$m, $W_{\mathrm{IR}} = 0.40\ \mu$m, and $R_{\mathrm{R}} = 5\ \mu$m.

were transferred from the photomask to the photoresist by deep ultraviolet photolithography ($\lambda = 193$ nm). After development, inductively coupled plasma etching was conducted to remove the unprotected top silicon layer, forming the rectangular shape silicon waveguide. After the remove of photoresist, 1-μm thick top silica cladding was deposited by plasma-enhanced chemical vapor deposition onto the silicon waveguide. Fig. 5(a) and (b) show the microscope images (× 1000) of the fabricated dual-concentric microring/racetrack resonators with radii of 5 μm, respectively.

A. Dual-Concentric Ring Resonator

Firstly, fabricated dual-concentric MRRs with parameters of $W_{\mathrm{B}} = 0.30\ \mu$m, $G_{\mathrm{BR}} = 0.40\ \mu$m, $W_{\mathrm{OR}} = 0.40\ \mu$m, $G_{\mathrm{RR}} = 0.40\ \mu$m, $W_{\mathrm{IR}} = 0.40\ \mu$m, $R_{\mathrm{R}} = 5\ \mu$m are characterized. Due to the bandwidth limitation of adopted vertical grating coupler and measurement error, the measured transmission spectrum of dual-concentric MRR is calibrated by subtracting the loss induced by the grating coupler. As shown in Fig. 6, the insertion loss is around 5 dB within the interested wavelength range. Five resonances with the FSR ∼20 nm can be observed within the wavelength range from 1500 to 1600 nm.

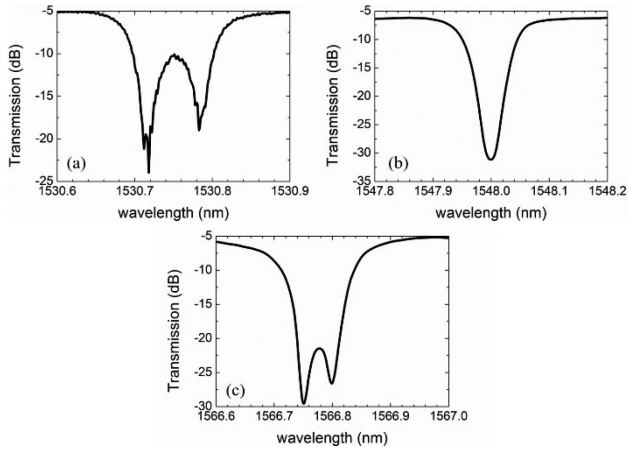

Fig. 7. Measured transmission spectrum as a function of optical wavelength, when $W_{\mathrm{B}} = 0.30\ \mu$m, $G_{\mathrm{BR}} = 0.40\ \mu$m, $W_{\mathrm{OR}} = 0.40\ \mu$m, $G_{\mathrm{RR}} = 0.40\ \mu$m, $W_{\mathrm{IR}} = 0.40\ \mu$m, and $R_{\mathrm{R}} = 5\ \mu$m. The transmission spectrum at the resonance wavelength (a) 1530.75 nm, (b) 1547.987 nm, and (c) 1566.78 nm.

Accompanying with the resonance wavelength variation, the resonance splitting changes, too. As shown in Fig. 7, the incomplete resonance splitting happens at 1530.75 nm. The total FWHM is ∼0.099 nm, while the maximum notch depth is ∼20 dB. At the resonance splitting wavelengths of 1530.718 and 1530.783 nm, corresponding FWHMs of 0.020 and 0.017 nm can be observed. Deduced Q factors are $\sim 7.65 \times 10^4$ and $\sim 9.00 \times 10^4$, respectively. In contrast, no splitting occurs at the resonance wavelength 1547.987 nm. Corresponding notch depth, FWHM, and Q factor are ∼26 dB, ∼0.050 nm and $\sim 3.10 \times 10^4$. An unremarkable resonance splitting happens at 1566.78 nm, which shows splitting resonance wavelengths of 1566.749 and 1566.799 nm. The maximum notch depth, total FWHM of resonance, and Q factor are ∼23 dB, 0.081 nm and $\sim 1.93 \times 10^4$.

Obviously, the resonance splitting differs at various wavelengths. According to the dispersion effect, the effective refractive index of waveguide relates to the interested wavelength. The mode field variation with the wavelengths leads to the change of evanescent field distribution, and the resulted mode coupling. Since u_{m} is determined by resonator parameters, the mutual-coupling accompanies with the introduction of inner-ring enhances the notch depth at the resonance wavelength. And the very possible overwhelmed mutual-coupling will lead to the resonance-splitting.

Compared to the simulation in Section III, the measured resonance around 1550 nm shows the same strength and no splitting occurs. However, the deviation of resonance wavelength and notch depth from the theoretical expectation can be observed in the measured transmission spectrum. This can be explained by the adopted FDTD method. In FDTD simulations, the target region is divided by millions of meshes (Yee cells), and then iterates forward from a source point over time based on the Maxwell equations. The accuracy strongly depends on the mesh size and the calculation time. The smaller mesh can improve the accuracy. However, it will cost much larger memory, which is a great challenge for the hardware. Besides, the adopted smaller mesh

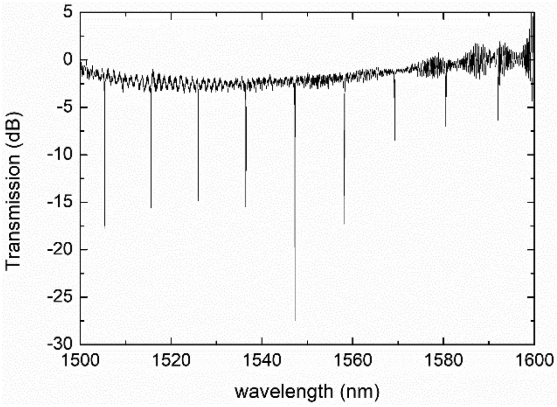

Fig. 8. Measured transmission spectrum of dual-concentric MRR as a function of optical wavelength at $W_{\rm b} = 0.40$ μm, $G_{\rm br} = 0.40$ μm, $W_{\rm or} = 0.40$ μm, $G_{\rm rr} = 0.52$ μm, $W_{\rm ir} = 0.30$ μm, $R_{\rm r} = 5$ μm and $L = 10$ μm.

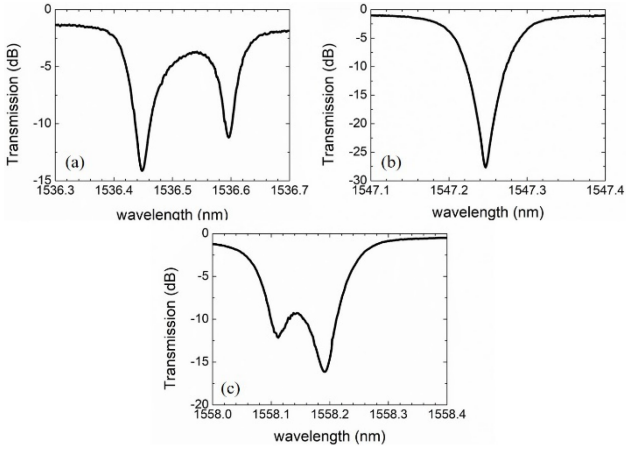

Fig. 9. Measured transmission spectrum as a function of wavelength around (a) 1536.50 nm, (b) 1547.247 nm, and (c) 1558.15 nm, when $W_{\rm b} = 0.40$ μm, $G_{\rm br} = 0.40$ μm, $W_{\rm or} = 0.40$ μm, $G_{\rm rr} = 0.52$ μm, $W_{\rm ir} = 0.30$ nm, $R_{\rm r} = 5$ μm and $L = 10$ μm.

would remarkably increase the simulation time, too. Therefore, the concession to mesh setup and 2D-FDTD simulation is used to reduce the time cost. These two compromises on calculation will inevitably affect the precision of coupling analysis, which results in the deviation of notch depth from the experimental results. The unavailable fabrication error contributes to the deviation, too. Nevertheless, the experimental results prove that the theoretical model could explain and anticipate the resonance splitting. It is suitable to describe the mutual coupling in the resonant process.

B. Dual-Concentric Racetrack Resonator

Similar experimental verification has been conducted to the dual-concentric racetrack resonator to compare with the theoretical expectation. A dual-concentric racetrack ring resonator with parameters of $W_{\rm b} = 0.40$ μm, $G_{\rm br} = 0.40$ μm, $W_{\rm or} = 0.40$ μm, $G_{\rm rr} = 0.52$ μm, $W_{\rm ir} = 0.30$ μm, $R_{\rm r} = 5$ μm and $L = 10$ μm has been fabricated. Fig. 8 shows the measured transmission spectrum within the wavelength range from 1500 to 1600 nm. Similar transmission to that of the dual-concentric MMR can be observed. Since FSR varies inversely with the circumference of ring/racetrack, different from the transmission spectrum in Fig. 6, nine resonance notches with FSR $\sim$11 nm can be observed in Fig. 8.

As shown in Fig. 9(a), the incomplete resonance splitting happens at the wavelengths of 1536.448 and 1536.596 nm. The total FWHM of resonance is $\sim$0.194 nm, while the maximum notch depth is $\sim$13 dB. FWHMs of splitting resonance are $\sim$0.029 and $\sim$0.021 nm. Q factors are calculated to be $\sim 5.30 \times 10^4$ and $\sim 7.32 \times 10^4$, respectively. However, no splitting occurs at the resonance wavelength 1547.247 nm. Corresponding notch depth, FWHM, and Q factor are $\sim$27 dB, $\sim$0.032 nm and $\sim 4.84 \times 10^4$, as shown in Fig. 9(b). In Fig. 9(c), the incomplete resonance splitting happens around 1558.15 nm. Two splitted resonances can be found at 1558.112 and 1558.191 nm. The maximum notch depth, total FWHM and Q factor are $\sim$15 dB, $\sim$0.121 nm and $\sim 1.29 \times 10^4$, respectively. Similar to the analysis in Section IV. The fabricated dual-concentric racetrack resonator shows almost the same resonance strength to that in Section III. Though only part simulated devices have been fabricated due to the fabrication limit, the obtained experimental results have already proved the working of our proposed model.

To be noted, many MRRs with quality factors above 10^6 have been reported [34]–[36]. However, the main purpose of this work is to investigate and adjust the resonance splitting in dual-concentric MRR and racetrack resonator. It is well known that Q factor is proportional to the radius, which implies high Q factor can be obtained in the price of size. Since a smaller footprint is more profitable, MRR with a small radius, such as 5 μm, is adopted in this work for compactness. And the reported Q factor for the compact size is deserved to be improved, too. In Ref. [14], the MRR with a radius of 5 μm has trapezoidal silicon pillars, exhibiting an applicable Q factor of 1.15×10^4. The Q factor is about 1.90×10^4 when the MRR works together with local weak gratings [15]. For the dual MRR in Ref. [16], the Q factor of the inner ring with a radius of 5 μm is around 3.70×10^4. In comparison, proposed dual-concentric MRR in this work shows a Q factor around 9.00×10^4 at 1530.783 nm. Supposing better fabrication, Q factor of proposed design may be further improved.

In most occasions, the resonance splitting in the dual-concentric MRR is supposed to be suppressed. In this work, the Q factor of dual-concentric MRR with a radius of 5 μm has been enhanced through the restrain of resonance splitting. This design has potentials in the applications of compact, high-sensitivity sensing, narrow-band filtering and lasers. On the other side, the resonance-splitting also can be strengthened, which could cover the unoccupied frequencies. New components, such as dual-wavelength laser and high-speed modulator can be developed.

V. Conclusion

In conclusion, we firstly implement the theoretical analysis to explain the asymmetric resonance splitting happened in dual-concentric ring resonators by coupled mode theory. 2D-FDTD simulations are conducted to predict and adjust the resonance splitting happened under different conditions. The characterization of fabricated dual-concentric MRR and

racetrack resonator proves that the asymmetry of resonance splitting can be tuned by adjusting the distance between the inner- and outer-ring, as well as the waveguide width. The notch depth improvement over 20 dB has been demonstrated on the 5-μm-radius double-ring structure.

REFERENCES

[1] H. Yi *et al.*, "Dual-microring-resonator interference sensor," *Appl. Phys. Lett.*, vol. 95, Dec. 2009, Art. no. 191112.

[2] G. D. Kim *et al.*, "Silicon photonic temperature sensor employing a ring resonator manufactured using a standard CMOS process," *Opt. Exp.*, vol. 18, pp. 22215–22221, Oct. 2010.

[3] W. Hong, G. Gu, and Q. Chen, "Analysis of microring filter with two embedded microring," *Optik*, vol. 124, pp. 3933–3935, Oct. 2013.

[4] D. Liu, C. Zhang, D. Liang, and D. Dai, "Submicron-resonator-based add-drop optical filter with an ultra-large free spectral range," *Opt. Exp.*, vol. 27, pp. 416–422, Jan. 2019.

[5] C. Zhang *et al.*, "Wavelength-selective 2 $\times$ 2 optical switch based on a $Ge_2Sb_2Te_5$-assisted microring," *Photon. Res.*, vol. 8, pp. 1171–1176, Jul. 2020.

[6] W. Chen *et al.*, "Silicon-based flexible-grid mode- and wavelength-selective switch utilizing microring resonators and Y-junctions," *J. Lightw. Technol.*, vol. 38, pp. 4000–4008, Aug. 2020.

[7] X. Guo, T. Dai, B. Chen, Y. Wang, and J. Yang, "An ultra-compact 4 $\times$ 4 and 8 $\times$ 8 optical switch based on dual-microring resonators," *IEEE Photon. Technol. Lett.*, vol. 32, no. 21, pp. 1365–1368, Nov. 2020.

[8] M. Mohsin, D. Schall, M. Otto, B. Chmielak, S. Suckow, and D. Neumaier, "Towards the predicted high performance of waveguide integrated electro-refractive phase modulators based on graphene," *IEEE Photon. J.*, vol. 9, no. 1, Feb. 2017, Art. no. 7800507.

[9] W. Shan *et al.*, "Broadband continuously tunable microwave photonic delay line based on cascaded silicon microrings," *Opt. Exp.*, vol. 29, pp. 3375–3385, Jan. 2021.

[10] D. Lin *et al.*, "A tunable optical delay line based on cascaded silicon nitride microrings for Ka-band beamforming," *IEEE Photon. J.*, vol. 11, no. 5, Oct. 2019, Art. no. 5503210.

[11] W. Jian, Z. Shuang, and X. Cao, "Demonstration of microring-based WDM-compatible mode-division multiplexing on a silicon chip," in *Proc. CLEO: Appl. Technol.*, San Jose, California, USA, May 2018.

[12] Y. Tan *et al.*, "Silicon-based hybrid demultiplexer for wavelength- and mode-division multiplexing," *Opt. Lett.*, vol. 43, pp. 1962–1965, 2018.

[13] X. Cao *et al.*, "On-chip multi-dimensional 1 $\times$ 4 selective switch with simultaneous mode-/polarization-/wavelength-division multiplexing," *IEEE J. Quantum Electron.*, vol. 56, no. 5, Oct. 2020, Art. no. 8400608.

[14] Z. Wang *et al.*, "High quality factor subwavelength grating waveguide micro-ring resonator based on trapezoidal silicon pillars," *Opt. Lett.*, vol. 41, no. 14, pp. 3375–3378, 2016.

[15] S. Werquin, Y. D. Koninck, and P. Bienstman, "Ring resonators with vertically coupling grating for densely multiplexed applications," *IEEE Photon. Technol. Lett.*, vol. 27, no. 1, pp. 97–100, Jan. 2015.

[16] L. A. M. Barea *et al.*, "Enhanced Q with internally coupled microring resonators," in *Proc. CLEO: Appl. Technol.*, San Jose, California, USA, Jun. 2013.

[17] X. Li *et al.*, "Sensitive label-free and compact biosensor based on concentric silicon-on-insulator microring resonators," *Appl. Opt.*, vol. 48, pp. F90–F94, Sep. 2009.

[18] B. Shen *et al.*, "Reconfigurable frequency-selective resonance splitting in chalcogenide microring resonators," *ACS Photon.*, vol. 7, pp. 499–511, Jan. 2020.

[19] D. Cai *et al.*, "High Q-factor microring resonator wrapped by the curved waveguide," *Sci. Rep.*, vol. 5, May 2015, Art. no. 10078.

[20] M. Moresco *et al.*, "Method for characterization of Si waveguide propagation loss," *Opt. Exp.*, vol. 21, pp. 5391–5400, Mar. 2013.

[21] Z. Zhang *et al.*, "Resonance-splitting and enhanced notch depth in SOI ring resonators with mutual mode coupling," *Opt. Exp.*, vol. 16, pp. 4621–4630, Mar. 2008.

[22] Q. Li *et al.*, "Fast light in silicon ring resonator with resonance-splitting," *Opt. Exp.*, vol. 17, pp. 933–940, Jan. 2009.

[23] G. C. Ballesteros, J. Matres, J. Martí, and C. J. Oton, "Characterizing and modeling backscattering in silicon microring resonators," *Opt. Exp.*, vol. 19, pp. 24980–24985, Dec. 2011.

[24] S. Tallur and S. A. Bhave, "Rayleigh scattering boosted multi-GHz displacement sensitivity in whispering gallery opto-mechanical resonators," *Opt. Exp.*, vol. 21, pp. 27780–27788, Nov. 2013.

[25] R. L. Chao, Z. Ahmad, J. Chen, Y. Lai, Y. Hung, and J. W. Shi, "Microring optical phase-shifters with low driving-voltage, low insertion loss, and small residual amplitude modulation," *J. Lightw. Technol.*, vol. 39, pp. 7740–7747, Dec. 2021.

[26] H. L. R. Lira, S. Manipatruni, and M. Lipson, "Broadband hitless silicon electro-optic switch for on-chip optical networks," *Opt. Exp.*, vol. 17, pp. 22271–22280, Dec. 2009.

[27] N. Sherwood-Droz *et al.*, "Optical 4 $\times$ 4 hitless silicon router for optical networks-on-chip (NoC)," *Opt. Exp.*, vol. 16, pp. 15915–15922, Sep. 2008.

[28] W. G. Jiang, Y. D. Zhang, F. X. Zhu, Y. Guo, and G. Yi, "Regulation of fast and slow light characteristics of the add-drop ring-resonator employing an assisted ring," *Opt. Exp.*, vol. 29, pp. 5141–5151, Feb. 2021.

[29] L. Liu *et al.*, "Compact and broadband optical add-drop de-multiplexer with cascaded elliptical micro-rings on SOI," *IEEE Photon. Technol. Lett.*, vol. 31, no. 6, pp. 451–454, Mar. 2019.

[30] J. C. C. Mak, A. Bois, and J. K. S. Poon, "Programmable multiring butterworth filters with automated resonance and coupling tuning," *IEEE J. Sel. Topics Quantum*, vol. 22, no. 6, Nov./Dec. 2016, Art. no. 4402909.

[31] A. Li, T. V. Vaerenbergh, P. D. Heyn, P. Bienstman, and W. Bogaerts, "Backscattering in silicon microring resonators: A quantitative analysis," *Laser Photon. Rev.*, vol. 10, pp. 420–431, Apr. 2016.

[32] B. E. Little, S. T. Chu, H. A. Haus, J. Foresi, and J. -P. Laine, "Microring resonator channel dropping filters," *J. Lightw. Technol.*, vol. 15, no. 6, pp. 998–1005, Jun. 1997.

[33] L. Sun *et al.*, "Design and optimization of silicon concentric dual-microring resonators for refractive index sensing," *Opt. Commun.*, vol. 395, pp. 212–216, Jul. 2017.

[34] Y. Zhang *et al.*, "Design and demonstration of ultra-high-Q silicon microring resonator based on a multi-mode ridge waveguide," *Opt. Lett.*, vol. 43, pp. 1586–1589, Apr. 2018.

[35] T. H. Chang, B. M. Fields, M. E. Kim, and C. L. Hung, "Microring resonators on a suspended membrane circuit for atom-light interactions," *Optica*, vol. 6, pp. 1203–1210, Sep. 2019.

[36] H. Qiu *et al.*, "A continuously tunable sub-gigahertz microwave photonic bandpass filter based on an ultra-high-Q silicon microring resonator," *J. Lightw. Technol.*, vol. 36, pp. 4312–4318, Oct. 2018.